УДК 533.6.013

DESIGN AND FLIGHT PERFORMANCE ANALYSIS OF ZENGZHANG-1 3D-PRINTED GEOPHYSICAL ROCKET

Runchen Gao
master`s student of the Department of Physics and Aerospace Technologies
Belarusian State University

Faxin Shen
PhD student of the Radio Astronomy and VLBI Research Group
Yunnan Observatories, Chinese Academy of Sciences

A. A. Spiridonov
Candidate of Physical and Mathematical Sciences
Belarusian State University

The design and results of a numerical analysis of the flight of the two-stage modular geophysical rocket Zengzhang-1 are presented. The flight dynamics analysis of the rocket (length 1795 mm, diameter 131 mm, mass 8797 g) for a given thrust profile of the L2200G rocket engine yielded estimated maximum parameters: flight altitude 3078 m, velocity 493 m/s (Mach 1.46), and acceleration 377 m/s². The rocket's layout and use of fins ensure a positive static margin and its controllability during both the powered ascent and ballistic flight phases. Simulation of the rocket's angular motion demonstrated that the flight occurs vertically, with minimal aerodynamic drag throughout the entire flight phase up to separation.

Keywords: Geophysical rocket, 3D printing technologies, stability margin, rocket flight dynamics.

Introduction

Geophysical rockets are crucial for aerospace research, offering an affordable way to access suborbital flight for atmospheric studies, microgravity experiments, and technology validation [1]. They are cost-effective, easy to operate, and deploy rapidly, making them ideal for education and science. Small-scale rockets, particularly in academia, allow students to engage in the full design-to-recovery cycle and provide a platform for testing flight technologies [2]. Programs like NASA's Student Launch and ESA's REXUS/BEXUS highlight their value in practical learning. Additive manufacturing, especially 3D printing, has revolutionized rocket production. Unlike traditional methods using expensive aluminum or composite laminates, 3D printing enables rapid, low-cost prototyping of complex geometries, perfect for educational and research rockets [3].

This study introduces a novel, low-cost geophysical rocket designed to reach 3 km altitude with a scientific payload. Its key innovations include being entirely 3D-printed from PETG, a modular two-section design for payload and propulsion, a dual-bay parachute recovery system, and achieving supersonic flight despite material constraints.

This work aims to guide future low-cost geophysical rocket projects and advance additive manufacturing in aerospace education and research.

Rocket Design

a) Modular Configuration

The rocket employs a two-section modular architecture. The forward module houses the payload and parachute bay, while the aft module contains the propulsion system. These are connected by a 60 mm coupler, which ensures both structural rigidity and ease of assembly. This design philosophy offers several advantages: flexibility in mission payload integration, improved safety during recovery by separating payload from propulsion, and enhanced manufacturability since modules can be independently 3D-printed. The vehicle measures 1795 mm in total length with a 131 mm diameter and has a gross mass of 8749 g. The payload bay is 300 mm long and 125 mm in diameter, capable of accommodating sensors or small experimental devices. Mass distribution between the payload and propulsion sections was carefully considered to balance the center of gravity (CG) and center of pressure (CP) for stable flight.

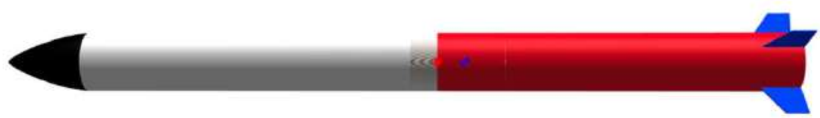

Figure 1 - ZZ-1 rocket model

b) Propulsion System

The L2200G solid rocket motor was selected as the propulsion system. Key specifications are total impulse of ~5104 Ns, average thrust of 2200 N, peak thrust of 2519 N, and a burn duration of ~2.3 s. With a gross mass of 4.78 kg and propellant mass of 2.52 kg, the motor provides a thrust-to-weight ratio exceeding 25, enabling rapid acceleration to supersonic speeds. The thrust profile is characterized by an initial sharp peak followed by sustained high thrust until burnout. This minimizes the influence of atmospheric turbulence near the ground. However, the extremely high acceleration of up to 38G imposes significant structural and payload survivability requirements. Additionally, thermal protection measures must be implemented to prevent PETG deformation near the motor casing [4].

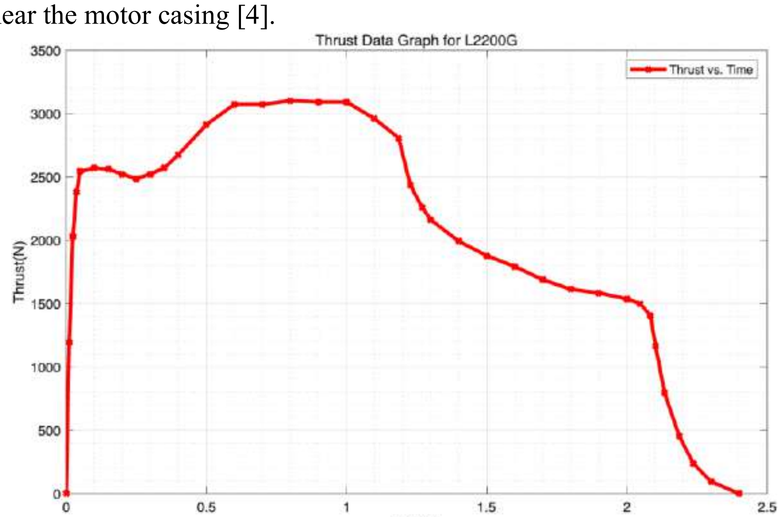

Figure 2 - Thrust data graph for L2200G solid rocket motor

c) Aerodynamic Design and Stability

Aerodynamic configuration plays a critical role in ensuring both stability and efficient flight performance. The rocket employs a Haack series nose cone, which is specifically designed to minimize drag. The Haack series family of nose cones is well-known for its ability to reduce wave drag in supersonic and transonic flight regimes. The shape parameter of the nose cone governs its drag-reducing properties, with a parameter of 0 producing a Von Karman nose cone (LD-Haack), ideal for minimizing drag for fixed length and diameter. In this design, we use a shape parameter of 0.333, which results in an LV-Haack nose cone, optimized to minimize drag for a fixed length and volume [5]. This design choice ensures that the rocket maintains a smooth and efficient flight trajectory at high speeds, particularly when crossing the transonic and supersonic regimes [6].

d) Material and Manufacturing

The rocket body is fabricated using PETG (Polyethylene Terephthalate Glycol-modified), with an assumed density of 1.25 g/cm³, like PLA. PETG was selected due to its superior thermal and mechanical properties compared to PLA while maintaining compatibility with standard FDM 3D printing. Its higher glass transition temperature (~80 °C) and improved impact resistance make PETG more suitable for small rockets subjected to high acceleration and motor exhaust heating [7, 8].

e) Recovery System

A dual-bay recovery system was adopted. Both the payload bay and propulsion section deploy independent 2500 mm parachute made of ripstop nylon (67 g/m²) with twelve shroud lines of 1200 mm length each. This configuration improves reliability by ensuring partial deceleration even if one parachute fails. Furthermore, separating the payload from the motor section enhances safety and reduces the risk of impact damage.

Dynamic Analysis of the Rocket

a) Rocket Coordinate System Definition

In rocket dynamics modeling, the following coordinate systems are mainly used, as shown in Figure 5 and Figure 6.

(1) Geodetic coordinate system S_D $(O_D X_D Y_D Z_D)$:

The celestial northeast coordinate system is used. The origin O_D is taken as the projection of the rocket launch point on the ground. The $O_D X_D$ axis points to the north of the launch point. The $O_D Y_D$ axis is vertical to the ground and is positive upward. The $O_D Z_D$ axis points to the east of the launch point. Without considering the rotation of the earth, this coordinate system is regarded as an inertial coordinate system.

(2) Carried geodetic coordinate system S_d $(O_d X_d Y_d Z_d)$:

The origin O_d is taken as the center of mass of the rocket. The coordinate axes $O_d X_d$, $O_d Y_d$, and $O_d Z_d$ are parallel to $O_D X_D$, $O_D Y_D$, and $O_D Z_D$ of the geodetic coordinate system S_D.

(3) Rocket body coordinate system S_t $(O_t X_t Y_t Z_t)$:

The origin O_t is taken as the center of mass of the rocket, the $O_t X_t$ axis points to the nose cone along the longitudinal axis of the rocket body, the $O_t Y_t$ axis is located in the rocket symmetry plane and is perpendicular to the O_tX_t axis, the O_tZ_t axis is perpendicular to the rocket symmetry plane and conforms to the right-hand rule with the O_tX_t axis and the O_tY_t axis.

(1) Airflow coordinate system S_q *($O_qX_qY_qZ_q$)*:

The origin O_q is taken as the center of mass of the rocket, the O_qX_q axis is along the rocket's airspeed G vector $\vec{U}$, the O_qY_q axis is located in the rocket symmetry plane and is perpendicular to the O_qX_q axis, and the O_qZ_q axis conforms to the right-hand rule with the O_qX_q axis and the O_qY_q axis.

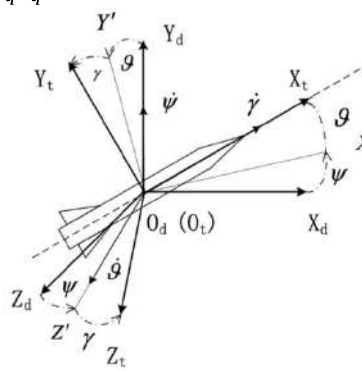

Figure 4 - The conversion relationship between the S_d and S_t

The relationship between the carried geodetic coordinate system S_d and the rocket body coordinate system S_t is determined by three angles: pitch angle ϑ, yaw angle ψ, and roll angle γ. First, rotate the carried geodetic coordinate system S_d around the O_dY_d axis by angle ψ, transforming the coordinate system to $O_dX'Y_dZ'$. Then, rotate it around the O_dX'axis by angle ϑ, transforming the coordinate system to $O_dX_tY'Z'$. Finally, rotate it around the O_tX_t axis by angle γ, transforming the coordinate system to $O_tX_tY_tZ_t$. This completes the transformation from the carried geodetic coordinate system S_d to the rocket coordinate system S_t. The corresponding coordinate transformation matrix B_d^t is:

$$B_d^t = B_x(\gamma)B_z(\vartheta)B_y(\psi) =$$

$$\begin{bmatrix} cos\vartheta cos\psi & sin\vartheta & -cos\vartheta sin\psi \\ -cos\gamma sin\vartheta cos\psi + sin\gamma sin\psi & cos\gamma cos\vartheta & cos\gamma sin\vartheta sin\psi + sin\gamma cos\psi \\ sin\gamma sin\vartheta cos\psi + cos\gamma sin\psi & -sin\gamma cos\vartheta & -sin\gamma sin\vartheta sin\psi + cos\gamma cos\psi \end{bmatrix} \quad (1)$$

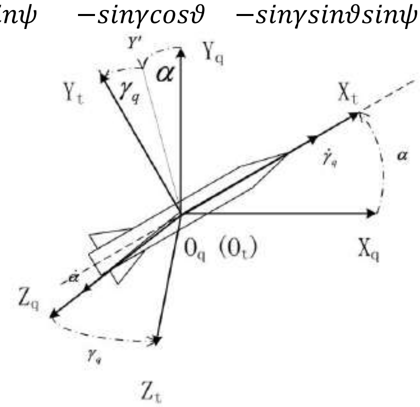

Figure 5 - The conversion relationship between the S_d and S_q

The relationship between the airflow coordinate system S_q and the rocket body coordinate system S_t is determined by the total angle of attack α and the longitudinal roll angle γ_q. First, the airflow coordinate system S_q is rotated by an angle α around the O_qZ_q axis to become the coordinate system $O_qX_tY'Z_q$. Then, the coordinate system is rotated by an angle γ_q around the O_qX_t axis to become the coordinate system $O_tX_tY_tZ_t$. This completes the transformation from the airflow coordinate system S_q to the rocket body coordinate system S_t. The corresponding coordinate transformation matrix B_q^t is:

$$B_q^t = B_x(\gamma_q)B_z(\alpha) = \begin{bmatrix} cos\alpha & sin\alpha & 0 \\ -sin\alpha cos\gamma_q & cos\alpha cos\gamma_q & sin\gamma_q \\ sin\alpha sin\gamma_q & -cos\alpha sin\gamma_q & cos\gamma_q \end{bmatrix} \quad (2)$$

b) Rocket Trajectory Equation

In flight, the rocket is affected not only by the engine thrust P acting on the center of mass and the gravity mg, but also by the aerodynamic force R. In the airflow coordinate system, the aerodynamic force R can be decomposed into the aerodynamic drag Q along the axial direction and the aerodynamic lift Y along the normal direction, that is :

$$R = [-Q\ Y\ 0] \quad (3)$$

$$Q = \frac{1}{2}C_x\rho v^2 S_M \quad (4)$$

$$Y = \frac{1}{2}C_y\rho v^2 S_M \quad (5)$$

Because the center of pressure of a rocket is generally not coincident with the center of mass, let the distance from the center of mass to the rocket nose cone be x_g, and the distance from the center of pressure to the rocket arrow cone be x_p, so the distance between the center of mass and the center of pressure is L,

$$L = [x_g - x_p\ 0\ 0] \quad (6)$$

Therefore, the aerodynamic force will generate a torque M_q to make the rocket rotate around the center of mass

$$M_q = L \times (B_q^t R) \quad (7)$$

1) Centroid kinematics equation

In the carried geodetic coordinate system S_d, the rocket is affected by gravity, aerodynamic force and engine thrust, and the differential equation of center of mass motion is:

$$m\frac{d}{dt}\begin{bmatrix} v_{xd} \\ v_{yd} \\ v_{zd} \end{bmatrix} = \begin{bmatrix} 0 \\ -mg \\ 0 \end{bmatrix} + B_t^d B_q^t \begin{bmatrix} -Q \\ Y \\ 0 \end{bmatrix} + B_t^d \begin{bmatrix} P \\ 0 \\ 0 \end{bmatrix} \quad (8)$$

2) Rotational kinematics equation

In the rocket body coordinate system S_t, the kinematics equation of the rocket rotating around the center of mass is:

$$\begin{cases} I_x \dfrac{d\omega_x}{dt} + \left(I_z - I_y\right)\omega_z\omega_y = M_{q,xt} \\ I_y \dfrac{d\omega_y}{dt} + (I_x - I_z)\omega_x\omega_z = M_{q,yt} \\ I_z \dfrac{d\omega_z}{dt} + \left(I_y - I_x\right)\omega_y\omega_x = M_{q,zt} \end{cases} \tag{9}$$

The rocket is a rotating body, so $I_y = I_z = I$, therefore

$$\begin{cases} I_x \dfrac{d\omega_x}{dt} = M_{q,xt} \\ I_y \dfrac{d\omega_y}{dt} + (I - I_z)\omega_x\omega_z = M_{q,yt} \\ I_z \dfrac{d\omega_z}{dt} + (I - I_x)\omega_y\omega_x = M_{q,zt} \end{cases} \tag{10}$$

1) System centroid kinematics equation

In the geodetic coordinate system S_D, the rocket's dynamic equations can be expressed as：

$$\frac{d}{dt}\begin{bmatrix} x_D \\ y_D \\ z_D \end{bmatrix} = \begin{bmatrix} v_{xD} \\ v_{yD} \\ v_{zD} \end{bmatrix} = \begin{bmatrix} v_{xd} \\ v_{yd} \\ v_{zd} \end{bmatrix} = B_t^d \begin{bmatrix} u_{c,xt} \\ u_{c,yt} \\ u_{c,zt} \end{bmatrix} + \begin{bmatrix} wind_{xd} \\ wind_{yd} \\ wind_{zd} \end{bmatrix} \tag{11}$$

Among them, u_c is the airspeed value of the rocket's center of mass, $u_{c,xt}$, $u_{c,yt}$, $u_{c,zt}$ are the components of u_c in the rocket body coordinate system S_t. The relationship between rocket ground speed $\vec{V}$, airspeed $\vec{U}$, and wind speed $\vec{W}$ is:

$$\vec{U} = \vec{V} - \vec{W} \tag{12}$$

2) System rotation around the centroid kinematics equation

Based on the transformation relationship between the carried geodetic coordinate system S_d and the rocket body coordinate system S_t, the rotational angular velocity of the rocket relative to the carried geodetic coordinate system S_d is the sum of vectors ψ, ϑ, and γ, therefore:

$$\begin{bmatrix} \omega_x \\ \omega_y \\ \omega_z \end{bmatrix} = \begin{bmatrix} \dot{\gamma} \\ 0 \\ 0 \end{bmatrix} + B_x(\gamma)\begin{bmatrix} 0 \\ 0 \\ \dot{\vartheta} \end{bmatrix} + B_x(\gamma)B_z(\vartheta)\begin{bmatrix} 0 \\ \dot{\psi} \\ 0 \end{bmatrix} = \begin{bmatrix} 1 & sin\vartheta & 0 \\ 0 & cos\vartheta cos\gamma & sin\gamma \\ 0 & -cos\vartheta sin\gamma & cos\gamma \end{bmatrix}\begin{bmatrix} \dot{\gamma} \\ \dot{\psi} \\ \dot{\vartheta} \end{bmatrix} \tag{13}$$

Through matrix transformation, we can obtain:

$$\begin{bmatrix} \dot{\gamma} \\ \dot{\psi} \\ \dot{\vartheta} \end{bmatrix} = \begin{bmatrix} 1 & -cos\gamma tan\vartheta & sin\gamma tan\vartheta \\ 0 & \dfrac{cos\gamma}{cos\vartheta} & -\dfrac{sin\gamma}{cos\vartheta} \\ 0 & sin\gamma & cos\gamma \end{bmatrix}\begin{bmatrix} \omega_x \\ \omega_y \\ \omega_z \end{bmatrix} \tag{14}$$

By combining the above equations (8)-(14), the six-degree-of-freedom trajectory equation for rockets can be obtained [7,8].

Flight Performance Analysis

a) Flight Phases.

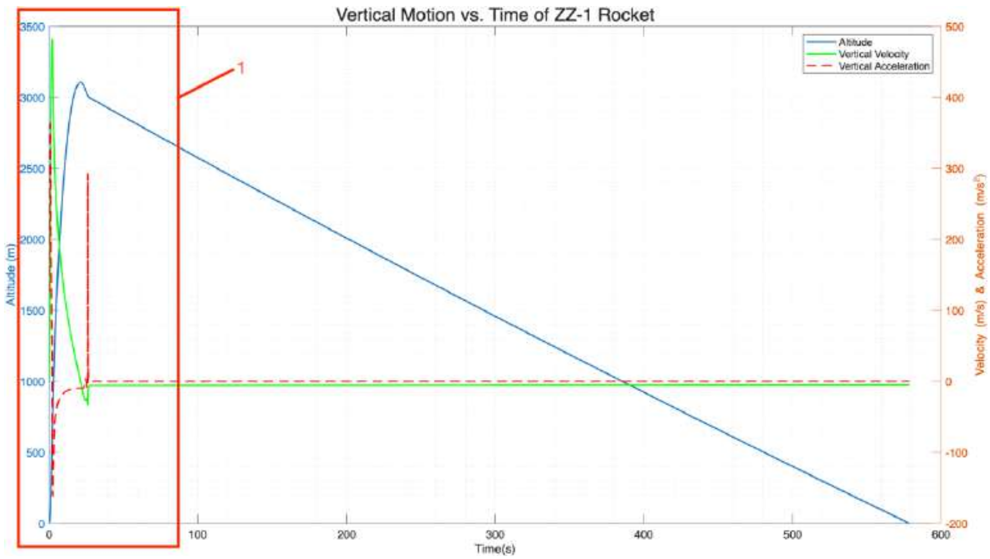

(a)

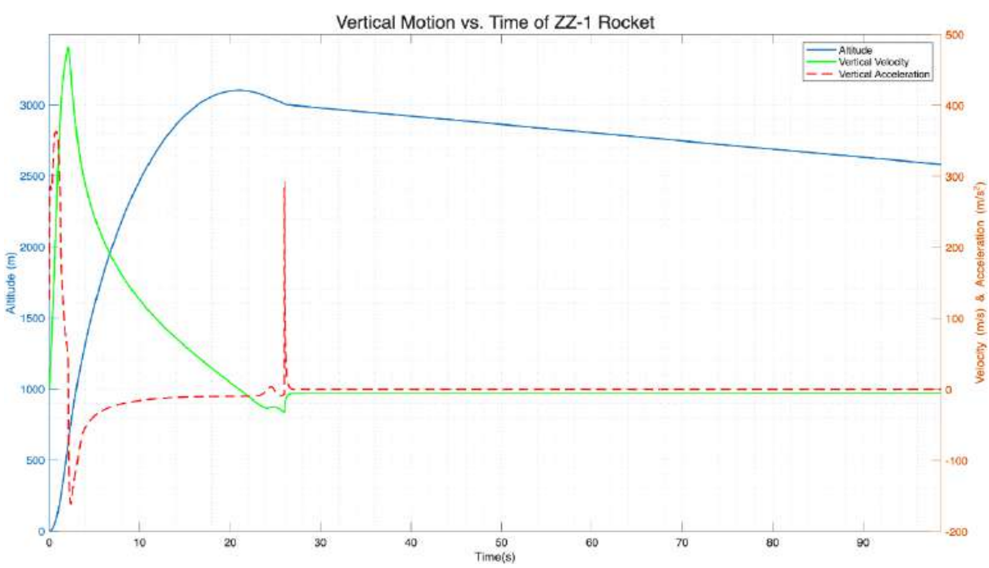

(b)

Figure 6 Vertical Motion parameters vs. Time of ZZ-1 rocket over a time interval (0, 600 s) of the entire flight (a) and during the rocket flight stage (0, 100 s) – region 1 (b)

The flight trajectory is divided into four phases:

1. Powered ascent (0 – 2.3s): Rapid acceleration under motor thrust, peaking at 377 m/s². Structural loads are highest in this phase.

2. Ballistic coast (2.3 – 20.7s): After burnout, the rocket coasts upward. Crossing the transonic regime, drag peaks, but aerodynamic shaping mitigates shock formation.

3. Apogee and separation (20.7s): At 3078m altitude, velocity decreases to near zero. The recovery system is deployed, separating the payload and motor sections.

4. Descent and landing (20.7s–touchdown): Both sections descend under parachutes, ensuring a safe landing with minimal impact energy.

b) Dynamic Analysis of Stability Margin During Flight

Although performance targets are met, the static margin of only 0.42 calibers indicates marginal stability. In turbulent or windy conditions, the rocket could experience significant pitch or yaw excursions. Improving aerodynamic stability through design adjustments will be essential for consistent real-world performance.

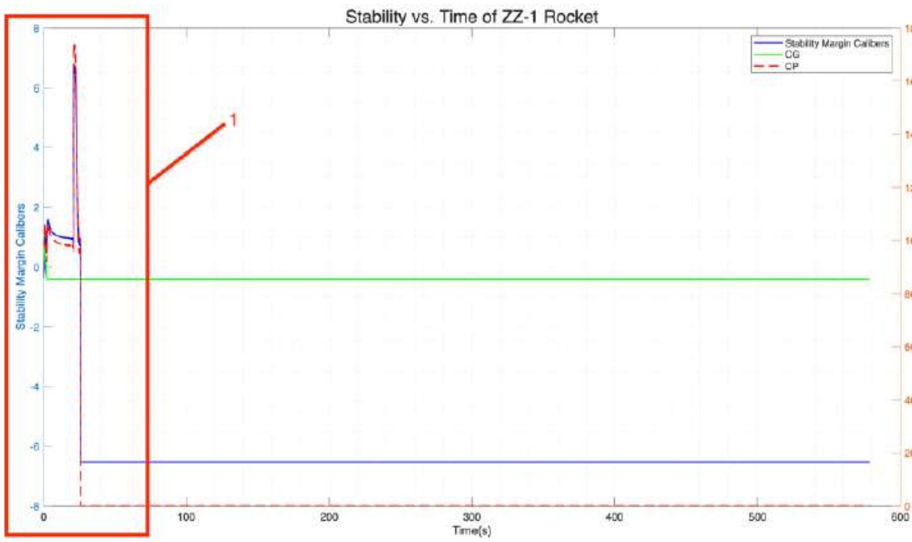

(a)

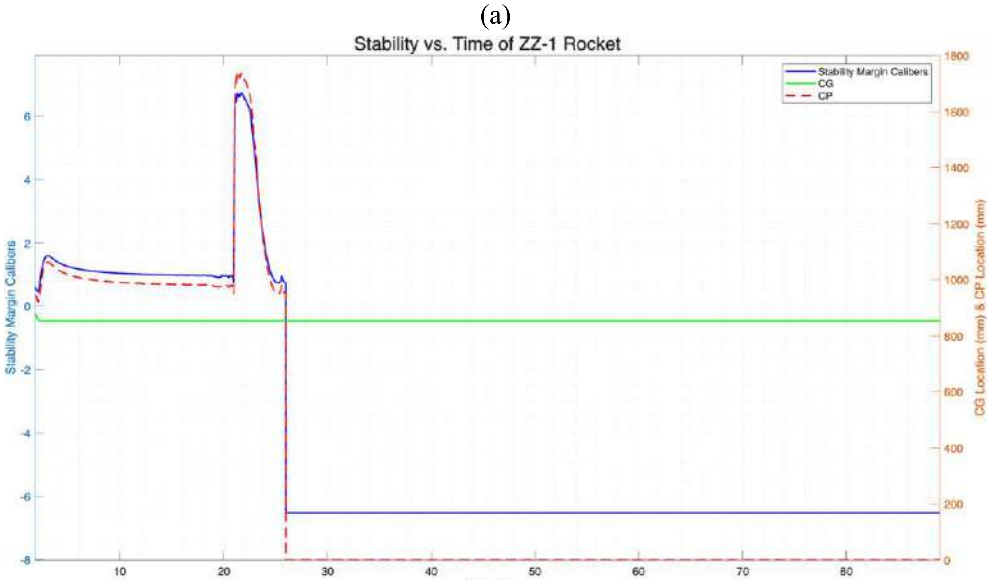

(b)

Figure 7 Stability vs. Time of ZZ-1 rocket over a time interval (0, 600 s) of the entire flight (a) and during the rocket flight stage (0, 90 s) – region 1 (b)

After the engine ignition, the stability margin (blue line) of the rocket rapidly increases from near zero, reaching a peak of approximately 1.4 radial lengths at about 2.5 seconds. This trend is typical: as the velocity increases, especially in the transonic region, the center of pressure (CP, red line) moves backward, increasing the distance from the center of gravity (CG, green line), resulting in an increase in stability margin. Subsequently, the margin slightly decreases and stabilizes at approximately 0.8 radial lengths until the engine shuts down. Throughout the entire powered flight phase, the stability margin remains positive, ensuring the controllability and attitude rigidity of the rocket under maximum dynamic pressure conditions [9,10].

c) Dynamic Analysis of Attitude During Flight

The rocket ignited and left the launch rail at approximately t = 1.5 s, entering the powered ascent phase. During this phase, the vehicle's vertical orientation (green curve) was stably maintained at 90°, indicating a near-perfect vertical trajectory and effective attitude hold. Concurrently, the angle of attack (blue curve), after a minor initial perturbation, rapidly converged to and remained near 0°. This provides strong evidence of the rocket's excellent longitudinal aerodynamic stability. This stability ensures that the vehicle flew with a minimal frontal cross-section through the region of maximum dynamic pressure, thereby reducing aerodynamic drag and enhancing flight efficiency [11,12].

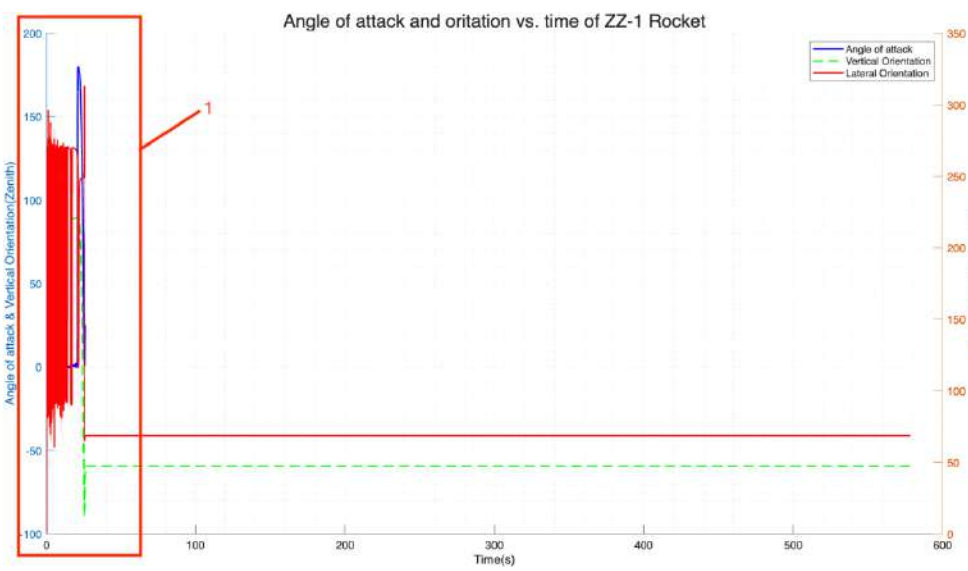

(a)

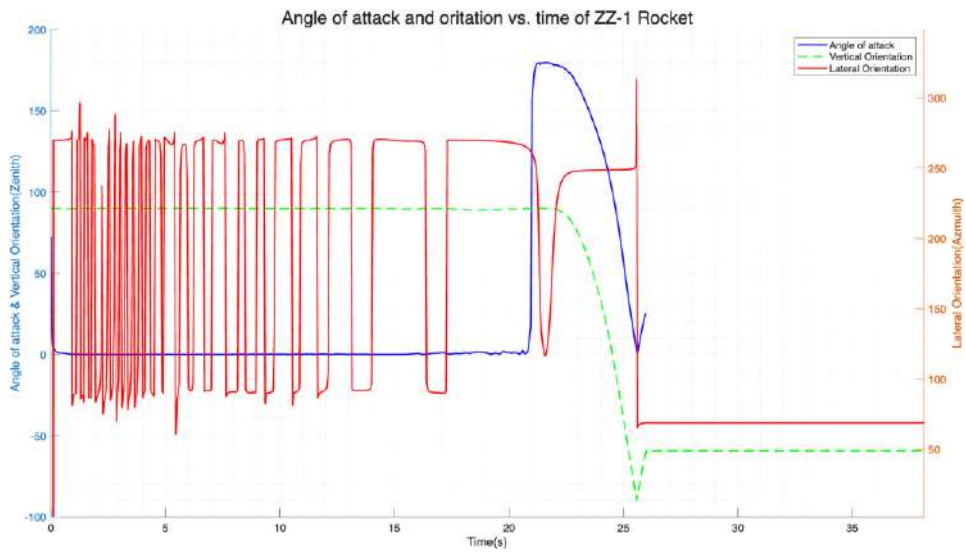

(b)

Figure 8 Angle of attack and orientation vs. time of ZZ-1 rocket over a time interval (0, 600 s) of the entire flight (a) and during the rocket flight stage (0, 40 s) – region 1 (b)

In contrast, the lateral orientation (red curve) exhibited violent, high-frequency oscillations during this phase, with the azimuth fluctuating rapidly between approximately 30° and 170°. This phenomenon indicates a significant roll anomaly while the motor was burning.

Conclusion

This study successfully demonstrates the comprehensive design and simulated flight performance of a geophysical rocket constructed entirely from PETG using additive manufacturing. The six-degree-of-freedom (6-DOF) flight simulation indicates the vehicle is capable of reaching an apogee of 3078 m and a peak velocity of 493 m/s (Mach 1.46), propelled by a maximum acceleration of 377 m/s² (38.4 G). These results provide strong theoretical evidence that 3D-printed PETG structures can withstand the significant aerodynamic and structural stresses inherent in transonic and supersonic flight regimes. Furthermore, the dynamic analysis confirmed positive flight stability throughout the critical powered ascent phase (0–2.3 s), with a static margin peaking at approximately 1.4 calibers. The simulation showed the vehicle's angle of attack converging rapidly to near-zero, validating the aerodynamic design's ability to maintain a stable, low-drag vertical trajectory. This modeling effort confirms the feasibility of the proposed modular architecture and material choice for demanding flight profiles. Building on this validated model, future work will prioritize the fabrication and empirical testing of a physical prototype. This vehicle will be integrated with an avionics suite to capture real-world flight data, which is essential for refining the simulation models presented herein. Additionally, research into advanced materials, such as carbon fiber reinforced plastics (CFRP), will be conducted to enhance structural and thermal performance for missions involving higher-thrust motors. In conclusion, this research establishes a robust design framework for the rapid and low-cost development of geophysical rockets, showcasing the significant potential of additive manufacturing to advance aerospace research and education.

LIST OF REFERENCES

1. ***Perkins, E. W.*** NACA RM A52H28: Theoretical Hap for Minimum Pre Me Drag Derived by Von Karman and by Haack / E. W. Perkins. – Washington : National Advisory Committee for Aeronautics, 1958. – 598 p.

2. NASA Sounding Rockets User Handbook / R.H. Burth [et al.] [Electronic resource]. – 2025. – URL: https://sites.wff.nasa.gov/code810/files/SRHB.pdf. (date of access: 11.09.2025).

3. ***Sutton, G. P.*** Rocket Propulsion Elements / G. P. Sutton, O. Biblarz. – New York : John Wiley & Sons, 2016. – 767 p.

4. ***Navarrete, L.*** Sounding Rockets: analysis, simulation and optimization of a solid propellant motor using Hopsan / L. Navarrete, P. Krus // Transportation Research Procedia. – 2018. – Vol. 29. – P. 255–267. doi: 10.1016/j.trpro.2018.02.023.

5. Integration validation of key components for small geophysical rockets / Y. Yun [et al.] // Aerospace Science and Technology. – 2020. – Vol. 100. – P. 105823. doi: 10.1016/j.ast.2020.105823.

6. ***Kumar, D.*** Design and Structural Analysis of Solid Rocket Motor Casing Hardware used in Aerospace Applications / D. Kumar, S. Nayana, S. Shree // Journal of Aeronautics & Aerospace Engineering. – 2016. – Vol. 5(2). – P. 1000166. doi: 10.4172/2168-9792.1000166.

7. Surface-Modified Electrospun Glass Nanofibers from Silane Treatment and Their Use for High-Performance Epoxy-Based Nanocomposite Materials / A. Mali [et al.] // Materials. – 2023. – Vol. 16. – P. 6817. doi: 10.3390/ma16206817.

8. ***Bista, N.*** Additive Manufacturing of Rocket Propulsion System: A Review. / N. Bista, S. A. Gampa, V. Dharaiya // Journal of Materials and Metallurgical Engineering. – 2022. – Vol. 12 (2). – P. 1–9. doi: 10.37591/JoMME.

9. Development of the Polish Small Sounding Rocket Program / A. Okninski [et al.] // Acta Astronautica. – 2015. – Vol. 108. – P. 46–56. doi: 10.1016/j.actaastro.2014.12.001.

10. ***Khan, M. A.*** Conceptual Design and Structural Analysis of Solid Rocket Motor Casing / M. A. Khan, B. K. Chaitanya, E. R. Cholleti // International Journal of Computational Engineering Science. – 2017. – Vol. 7(2). – P. 23–28.

11. ***Zipfel, P.*** Modeling and Simulation of Aerospace Vehicle Dynamics / P. Zipfel. – Reston : American Institute of Aeronautics and Astronautics, 2001. – 551 p. doi:10.2514/4.107535.

12. Aircraft control and simulation / B. L. Stevens, F. L. Lewis, E. N. Johnson. – New York : John Wiley & Sons, 2016. – 764 p.

Received by the editors on 02.12.2025

Contacts: rct.gaozh@bsu.by (Runchen Gao, Faxin Shen, Spiridonov Alexander Alexandrovich)

Гао Жуньчэнь, Шэнь Фасинь, Спиридонов А. А. **ПРОЕКТИРОВАНИЕ И АНАЛИЗ ЛЕТНЫХ ХАРАКТЕРИСТИК ГЕОФИЗИЧЕСКОЙ РАКЕТЫ ZENGZHANG-1, СОЗДАННОЙ ПО ТЕХНОЛОГИИ 3-D ПЕЧАТИ**

Представлены конструкция и результаты численного анализа движения двухступенчатой модульной геофизической ракеты Zengzhang-1. Анализ динамики полета ракеты длинной 1795 мм, диаметром 131 мм, массой 8797 г для заданного профиля силы тяги ракетного двигателя L2200G позволил оценить максимальные высоту полета 3078 м, скорость движения 493 м/с (1,46 Маха) и ускорение 377 м/с². Компоновка ракеты и применение стабилизаторов обеспечивает положительный запас устойчивости и ее управляемость на активном и баллистическом участках полета. Моделирование углового движения ракеты показало, что полет происходит вертикально с минимальным лобовым сопротивление на всем участке полета вплоть до разделения.

Ключевые слова: геофизическая ракета, технологии аддитивного производства, запас устойчивости, динамика полета ракеты.